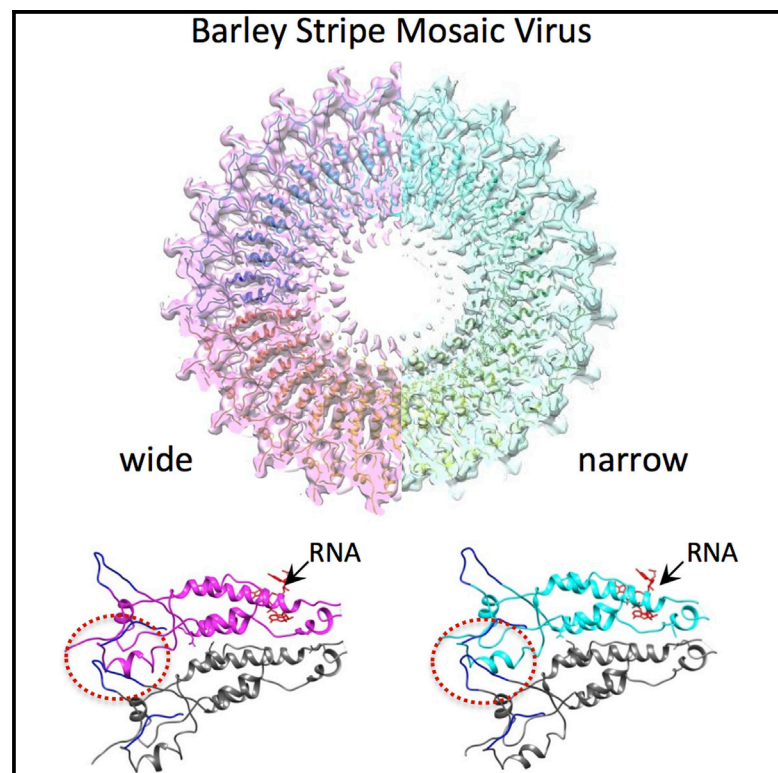# Novel Inter-Subunit Contacts in Barley Stripe Mosaic Virus Revealed by Cryo-Electron Microscopy

Graphical Abstract

Authors

Daniel Kofi Clare, Eugenia V. Pechnikova, Eugene V. Skurat, ..., Olga S. Sokolova, Andrey G. Solovyev, Elena V. Orlova

Correspondence

e.orlova@mail.cryst.bbk.ac.uk

In Brief

Clare et al. have determined the structure of barley stripe mosaic virus at 4.1 Å and found that there were two distinct virions. The authors have found a new lateral contact between the capsid proteins that is essential for virion stability.

Highlights

- Determined the near-atomic structure of barley stripe mosaic virus (BSMV)

- Two forms of BSMV were found, both of which are important for its life cycle

- Identified a new lateral contact that is essential for the stability of BSMV

- BSMV structure may offer an alternative to TMV in biotemplated materials

Accession Numbers

5a79
5a7a

Novel Inter-Subunit Contacts in Barley Stripe Mosaic Virus Revealed by Cryo-Electron Microscopy

Daniel Kofi Clare,[1] Eugenia V. Pechnikova,[2] Eugene V. Skurat,[3] Valentin V. Makarov,[4] Olga S. Sokolova,[2,3] Andrey G. Solovyev,[4] and Elena V. Orlova[1,*]

[1]Institute of Structural and Molecular Biology, UCL and Birkbeck, Malet Street, London WC1E 7HX, UK
[2]A.V. Shubnikov Institute of Crystallography RAS, 59 Leninsky Avenue, 119333 Moscow, Russia
[3]Department of Biology, Moscow State University, 1 Leninskie Gory, Building 12, 119991 Moscow, Russia
[4]A.N. Belozersky Institute of Physico-Chemical Biology, Moscow State University, 119992 Moscow, Russia
*Correspondence: e.orlova@mail.cryst.bbk.ac.uk
http://dx.doi.org/10.1016/j.str.2015.06.028

SUMMARY

Barley stripe mosaic virus (BSMV, genus *Hordeivirus*) is a rod-shaped single-stranded RNA virus similar to viruses of the structurally characterized and well-studied genus *Tobamovirus*. Here we report the first high-resolution structure of BSMV at 4.1 Å obtained by cryo-electron microscopy. We discovered that BSMV forms two types of virion that differ in the number of coat protein (CP) subunits per turn and interactions between the CP subunits. While BSMV and tobacco mosaic virus CP subunits have a similar fold and interact with RNA using conserved residues, the axial contacts between the CP of these two viral groups are considerably different. BSMV CP subunits lack substantial axial contacts and are held together by a previously unobserved lateral contact formed at the virion surface via an interacting loop, which protrudes from the CP hydrophobic core to the adjacent CP subunit. These data provide an insight into diversity in structural organization of helical viruses.

INTRODUCTION

Barley stripe mosaic virus (BSMV) is a single-stranded RNA (ssRNA) virus of genus *Hordeivirus* (family Virgaviridae) that infects many agriculturally important monocot species, including barley, oat, wheat, and maize (Jackson et al., 1989; Jackson and Lane, 1981; McKinney, 1951; Wiese, 1987). During the last few decades, BSMV has been extensively studied to determine the functions of viral proteins and their interaction with plant hosts (Jackson et al., 2009); however, its virion structure has remained unknown. The only viruses of the family Virgaviridae that are structurally characterized in atomic detail are viruses of the genus *Tobamovirus* (Table S1). They have a positive-sense ssRNA monopartite genome. The best characterized representative of this genus is tobacco mosaic virus (TMV), the structure of which was the first to be elucidated in atomic detail (Ge and Zhou, 2011; Namba et al., 1989; Stubbs et al., 1977). Later, a

number of other viruses of the same genus were observed in atomic detail by X-ray fiber diffraction (Pattanayek and Stubbs, 1992; Tewary et al., 2011; Wang and Stubbs, 1993, 1994). All structurally characterized members of the genus *Tobamovirus* revealed a conserved helical organization of virions, with a diameter of 180 Å and 16.3 subunits per turn with a helical pitch of 23 Å (Namba et al., 1989; Pattanayek and Stubbs, 1992; Stubbs et al., 1977; Tewary et al., 2011; Wang and Stubbs, 1993, 1994). However, without RNA, TMV coat protein (CP) forms double-layered cylindrical disks, with each disk containing 17 subunits (Bhyravbhatla et al., 1998; Butler, 1999), but the addition of RNA initiates the formation of helical TMV virions (Schon and Mundry, 1984). CPs that are responsible for protecting the genome by encapsidating it in rigid rod-like virions (Adams et al., 2011) are similar in size (∼17 kDa) in all known viruses of this genus and have virtually an identical fold. CP subunits in the virion are held together by the lateral and axial contacts, which make them very rigid.

BSMV belongs to the genus *Hordeivirus*, another genus of the family Virgaviridae, and, similar to TMV, has rod-like virions (Jackson et al., 2009). BSMV has a tripartite positive-sense ssRNA genome consisting of three RNAs termed α, β, and γ (Figure 1). All three RNAs are required for infection. The *Hordeivirus* genome encodes seven major proteins; three of them, the methyltransferase/helicase subunit of the replicase, the CP (∼23 kDa), and the polymerase subunit of the replicase, are translated directly from the viral genomic RNAs, while expression of movement proteins encoded by a triple gene block and a pathogenicity protein are mediated by subgenomic RNAs (Jackson et al., 2009). Electron microscopy (EM) of reaggregated BSMV CP demonstrated that it can form multiple assemblies: disks with ∼21 subunits per ring, rod-like aggregates (presumably stacked dicks), and rigid rods with helical packaging (Atabekov et al., 1968; Kiselev et al., 1966, 1969; Veerisetty, 1978). X-Ray fiber diffraction of the BSMV virions demonstrated their helical organization; however, the helical parameters of BSMV virions were different from those of TMV (Atabekov and Novikov, 1966, 1971; Finch, 1965; Kiselev et al., 1966). The BSMV helix was reported to have a pitch of ∼26 Å, a diameter of 210–230 Å, and a 30- to 40-Å-wide central channel (Finch, 1965). Stoichiometric estimations suggested that the virions have roughly 26 CP molecules per turn with the viral RNA organized helically at a radius of around 63 Å and each CP probably bound to three nucleotide
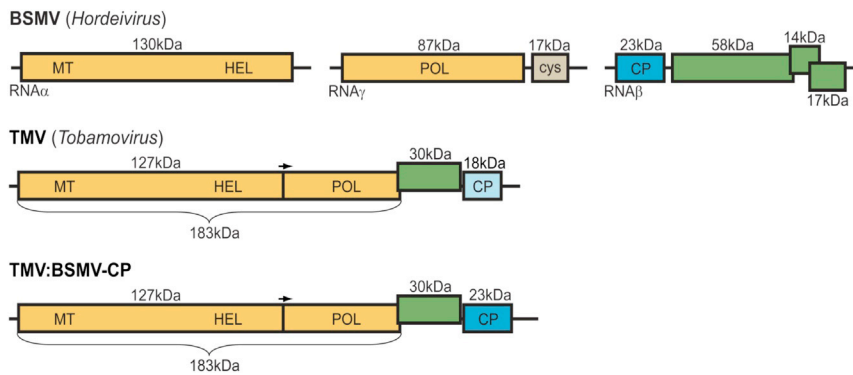
Figure 1. Schematic Representation of Genome Structures of BSMV, TMV, and TMV:BSMV-CP, A Recombinant TMV Carrying the BSMV CP Gene

Genes are shown as boxes and molecular masses of encoded proteins are indicated. Genes of replicative proteins are shown in yellow and the locations of conserved protein sequence domains of methyltransferase (MT), helicase (HEL), and polymerase (POL) are indicated. Movement protein genes coding for proteins necessary for viral cell-to-cell transport are shown in green. CP, capsid protein gene; cys, the gene of BSMV cysteine-rich protein involved in silencing suppression.

residues of encapsidated RNA (Veerisetty, 1978). Recent results from X-ray fiber diffraction and cryo-electron microscopy (cryo-EM) suggested that BSMV has a helical pitch of 25.8 ± 0.2 Å with 23.2 subunits per one helix turn with ssRNA located at radius of 50 Å (Kendall et al., 2013). The authors also proposed that the CPs of hordeiviruses and tobamoviruses have similar folds.

Here, we have used cryo-EM to determine the three-dimensional (3D) structure of the BSMV virions. We found for the first time that BSMV has two different virion types, the wide and the narrow, in both wild-type virions and chimeric virions formed by encapsidating TMV RNA with the BSMV CP (Figure 1). Our results confirm that the overall BSMV CP fold is similar to that of TMV with a number of key conserved residues in similar positions in both structures. However, we also found important differences in inter-subunit contacts between hordeivirus and tobamovirus virions: BSMV CP does not have axial contacts, in contrast to TMV CP, but BSMV does make a new high-radius lateral inter-subunit contact that is formed by an insertion, absent in tobamoviruses, that protrudes from the hydrophobic core of the CP toward the adjacent CP in the virion.

RESULTS

Overall Organization of BSMV Virions

We have analyzed a purified sample of the wild-type BSMV (wtBSMV), consisting of virions, which contain encapsidated genomic RNAs. To assess the helical parameters, images of the negatively stained virions were aligned and classified (see Supplemental Experimental Procedures). Then, the helical parameters were estimated using diffraction patterns from the best classes (Figure 2). Additional evaluation of helical parameters was done via assessment of the SD and contrast of 3D reconstructions (see Supplemental Experimental Procedures). From this, we found that BSMV has a helical pitch of 26.2 Å, with 111 subunits per period. For detailed structural determination, low-dose cryo-EM images of BSMV were taken. However, following standard image processing protocols (Clare and Orlova, 2010), it was difficult to obtain a map better than 7-Å resolution. Therefore, we checked the alignment quality using multivariate statistical analysis (MSA) (van Heel et al., 2000) and identified eigen images that suggested a variation in virion size (see Experimental Procedures; Figure S1) (Orlova and Saibil, 2010). Using these eigen images, we separated the images into two populations: the narrow and wide particles.

To understand if the multiple RNAs of the wtBSMV could account for existence of two types of virions, we analyzed images of chimeric BSMV (chBSMV), in which the single ssRNA of TMV has been coated with non-modified BSMV CP. The chimeric virions were produced in plants infected with the chimeric construct TMV:BSMV-CP (see Experimental Procedures; Figure 1). The chBSMV images were collected in both negative stain and cryo conditions. Diffraction patterns of the chBSMV did not differ from the wtBSMV and revealed the same helical parameters: a pitch of 26.2 Å, and 111 subunits/period. However, again using standard image processing procedures, we were not able to obtain a high-resolution map. MSA used after the alignment procedure indicated the presence of virions of different sizes similar to that of the wtBSMV. Again, the segments were separated according to their width into two populations: the narrow virion particles with a diameter of 216 Å and the wide virion particles with a diameter of 224 Å. Their helical parameters were estimated to be 106 and 111 subunits/period accordingly (Figure S2).

Separation of particles according to their width has allowed us to improve the map resolutions for the chBSMV virions to 4.1 Å for the narrow and wide virions (Figures 3 and 4; Figures S3 and S4). For the wtBSMV virions, the map resolutions were improved to 5.2 Å and 6.1 Å for the narrow and wide virions, respectively (Figures S3 and S4). Comparison of helical parameters for wtBSMV and chBSMV suggests that encapsidated viral RNA does not control the width of the BSMV virions. We have then used maps of ch- and wtBSMV virions in combination with homology modeling using I-Tasser (Roy et al., 2010), flexible fitting (Topf et al., 2008), and both manual and automatic refinement (see Experimental Procedures) to build an atomic model of the BSMV CP (Figures 3 and 4).

Position of CPs in BSMV and TMV

The main difference between BSMV and TMV sequences are three long insertions in BSMV, two of which form long loops: one is located in the inner channel (residues 141–152, which are not present in the cryo-EM density) and the other protrudes from the hydrophobic core close to the outer surface of the virion (residues 84–94) (Figures S5 and S6; Figure 5A). The third insertion is located at the N terminus (residues 1–10) and sits on top of the hydrophobic core of BSMV (Figure 5A). The CP structure is almost identical in the narrow and wide forms of BSMV (Figure 5B).

In the BSMV capsid, the lateral distance between BSMV CPs is ∼7 Å and is similar to that of the TMV CP (Figure 6 top,

A

Indexing BSMV

B **C** **D**

Values of Bessel function are in orange
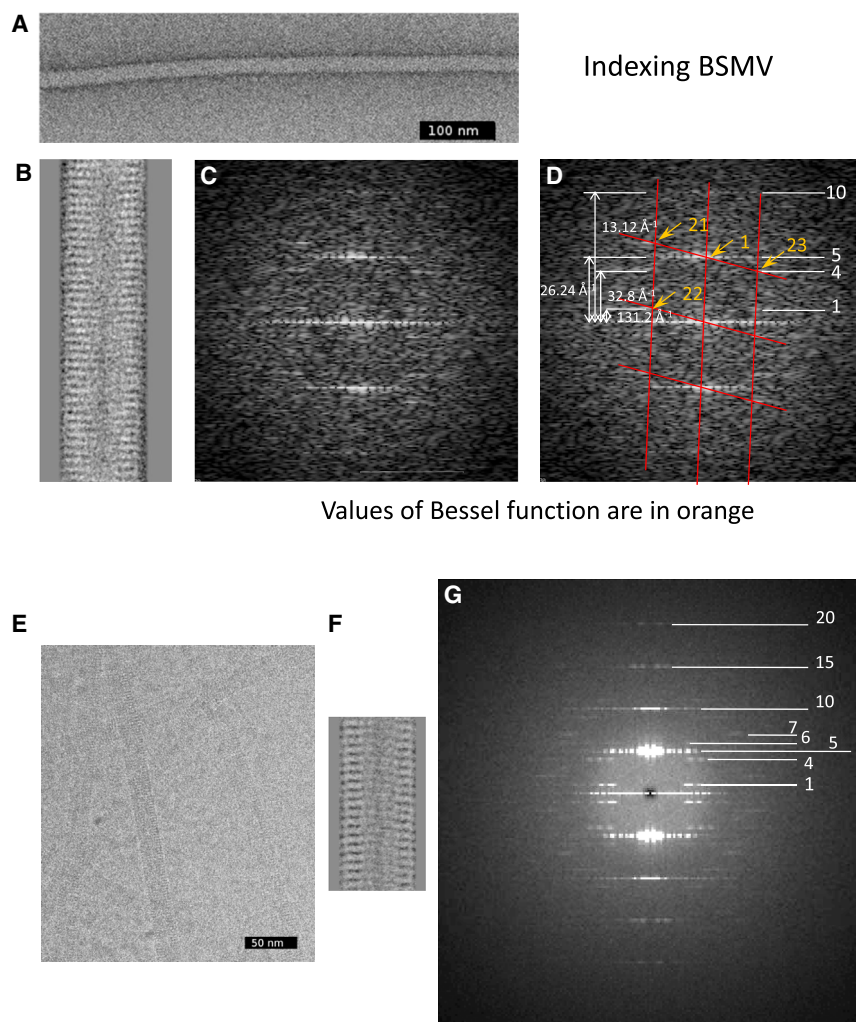
E **F** **G**

Figure 2. Determination of Helical Parameters of BSMV

(A) Image of BSMV in negative stain.
(B) Image of an average segment of wtBSMV.
(C) Diffraction pattern from the segment in (B).
(D) The diffraction pattern with the labeled layer lines and distances between reflections.
(E) Cryo image of BSMV.
(F) Segment class average of BSMV in cryo with its labeled diffraction pattern shown in (G).

CP Polypeptide Chain Fold

The overall fold of the BSMV CP is similar to that of TMV, cucumber green mottle mosaic virus (CGMMV), ribgrass mosaic virus (RMV), and hibiscus latent Singapore virus (HLSV). BSMV CP has a central core of four helices (Figure 5A; Figure S8), which have been labeled according to TMV nomenclature as RR, RS, LR, and LS (Figure 5A). The LR helix of BSMV is shorter than the equivalent helix in TMV. The BSMV CP has three small helices: two of them are located in the outer region and one is positioned close to the central channel of the virion. BSMV CP has a very similar arrangement of its small helices to that of TMV, as they are also located on the peripheral part of the CP and close to the central channel (Figure 5A).

Sequence alignment of TMV-like and BSMV-like viruses showed that there are a small number of residues that are conserved between them (14.6% aa sequence identity for TMV-BSMV alignment) (Figure 5A; Figure S5). All amino acids that are conserved between the *Tobamovirus* and *Hordeivirus* are located in similar positions in space when the structures of BSMV and TMV are superimposed. This is particularly true for the large aromatic side chains of the hydrophobic core that are conserved across most of the rod-like viruses (Figure 5A; Figure S5). These residues include Tyr14 (TMV:Tyr2), Trp33 (TMV:Trp17), Phe79 (TMV:Phe62), Phe98 (TMV:Tyr70 side chains point in opposite directions), Phe182 (TMV:Phe144), Leu188 (TMV:Leu150), and Trp190 (TMV:Trp152). This highlights that the overall CP fold is preserved even when only a small number of key residues are conserved. Additional aromatic amino acids near the core are conserved only in the more closely related viruses (BSMV:Trp19 and Trp32). There is also a residue that fluctuates in sequence but is conserved structurally in the hydrophobic core, Trp32 (TMV:Trp52). The other conserved residues are mainly charged residues and are involved in either RNA binding, such as Arg122 and Asp157 (TMV: Arg92 and Asp116), or in presumably important positions for fold stabilization such as Arg57, Arg78, Asp116, Glu125, and Glu183 (TMV:Arg41, Arg61, Asp88, Glu95, and Glu145) (Figure S5).
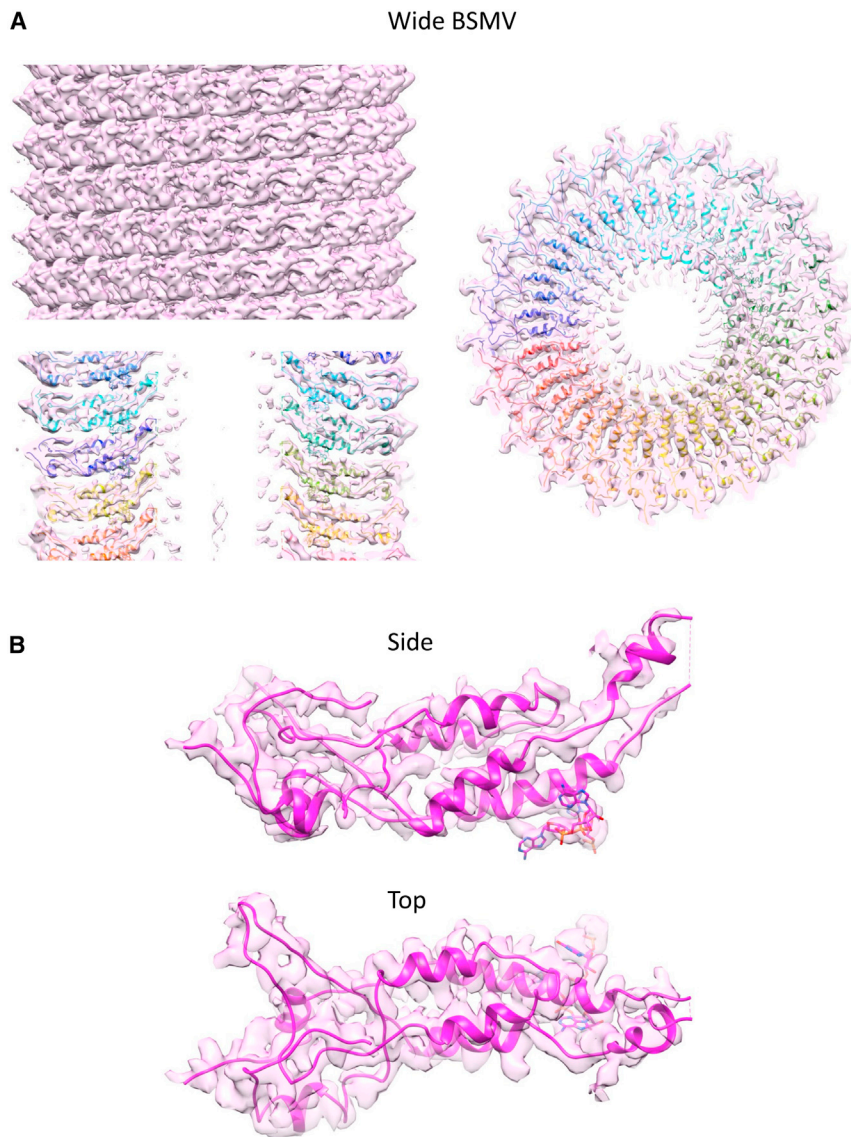
measured in the middle of the CP between equivalent residues in both BSMV and TMV located on the RR and LR helices of adjacent subunits). The tilts of the main body of the BSMV and TMV subunits, with respect to the plane perpendicular to the helical axis, are different. Subunits in the BSMV virions are more horizontal when compared with the TMV subunits (10° compared with 20°, Figure 6 side and Figure S7). However, the region of BSMV closest to the inner channel of the capsid is more tilted than in TMV (45° compared with 20°, Figure 6 side, Figure S7D). Another interesting observation is that the distance in the axial direction between BSMV CP is bigger by ~6 Å compared with that in TMV. The equivalent main chain elements in BSMV subunits are located 4–6 Å axially farther away than in TMV (Figure 6 side, Figure S7; measured in the middle of the CP between equivalent residues in BSMV and TMV). This increased axial subunit distance allows space for both the N-terminal insertion (aa 3–10) and the insertion loop (aa 84–94) extending from the hydrophobic core of BSMV. The insertion loop is directly involved into inter-subunit contacts (Figure 6 front). Both of the insertions in BSMV CP are located near the surface of the capsid and help seal the outer surface of the capsid from the environment (Figure 6 top, side, and front).

A

Wide BSMV

B

Side

Top

Figure 3. Wide chBSMV Reconstruction
(A) The wide BSMV virion (magenta) viewed from the outside (side), cut away (side), and top cut away. The map was filtered between 12 and 6 Å and the coordinates are shown as C-α only (rainbow colored).
(B) A single subunit cut out from the wide virion shown from the side and the top. The map (magenta surface) was filtered between 10 and 3.8 Å and atoms are shown in magenta.

main chain of Glu125 and not the side chain (see comment later about acidic residues). The cryo-EM density in this region is not as good as the density for the main helices and RNA binding site and thus makes the interpretation more difficult. Two lateral inter-subunit salt bridges are also present in TMV (Figure 6), CGMMV, RMV, and HLSV, but the ion pairs forming them vary between the different viruses (TMV/RMV Arg113-Asp115 and Arg122-Asp88; CGMMV Arg113-Asp115 and Arg77-Glu130; HLSV His122-Asp88 and Arg31-Glu81) (Tewary et al., 2011). It is possible that the reduced number of inter-subunit interactions in BSMV may explain its lower stability compared with TMV virions (Makarov et al., 2013).

The insertion loop (aa 84–94) protrudes from the hydrophobic core of BMSV CP and interacts with the adjacent lateral subunit on the outer surface of the virion (Figures 6C and 7C; Figure S6). This contact seems to be a combination of charged and hydrophobic residues and involves Tyr91, Ile86 from the loop, and Asp76, His13, and Lys9 from the next subunit. Specifically, Asp76 makes a contact with the ring of Tyr91, Lys9 makes a contact with the main chain of Tyr91, and His13 makes a contact with Ile86. His13 and Tyr91 are conserved in both the hordeiviruses and the pecluviruses. Ile86 is substituted with leucine in PLSV, LRSV, PCV, and IPCV-L, and Lys9 is either lysine in the other hordeiviruses or an arginine in IPCV (in PCV, the equivalent residue is a leucine). The residue conservation suggests that this contact will be the same in the hordeiviruses and similar in the pecluviruses.

To test whether the insertion loop forms an essential connection between BSMV CPs when in the virion, we constructed two mutants of the BSMV CP. In the first, CP-del10, aa 84–94 were deleted; and in the second, CP-IY/GG, Ile86 and Tyr91, which form the contact with neighboring CP subunit, were replaced with Gly residues (Figure 8; Figures S5 and S6). Chimeric viruses carrying the mutant CP genes were able to systematically infect *Nicotiana benthamiana* plants and accumulated to levels similar to that of chBSMV (Figure 8; see Experimental Procedures). However, virions were not found in chBSMV-del10- or
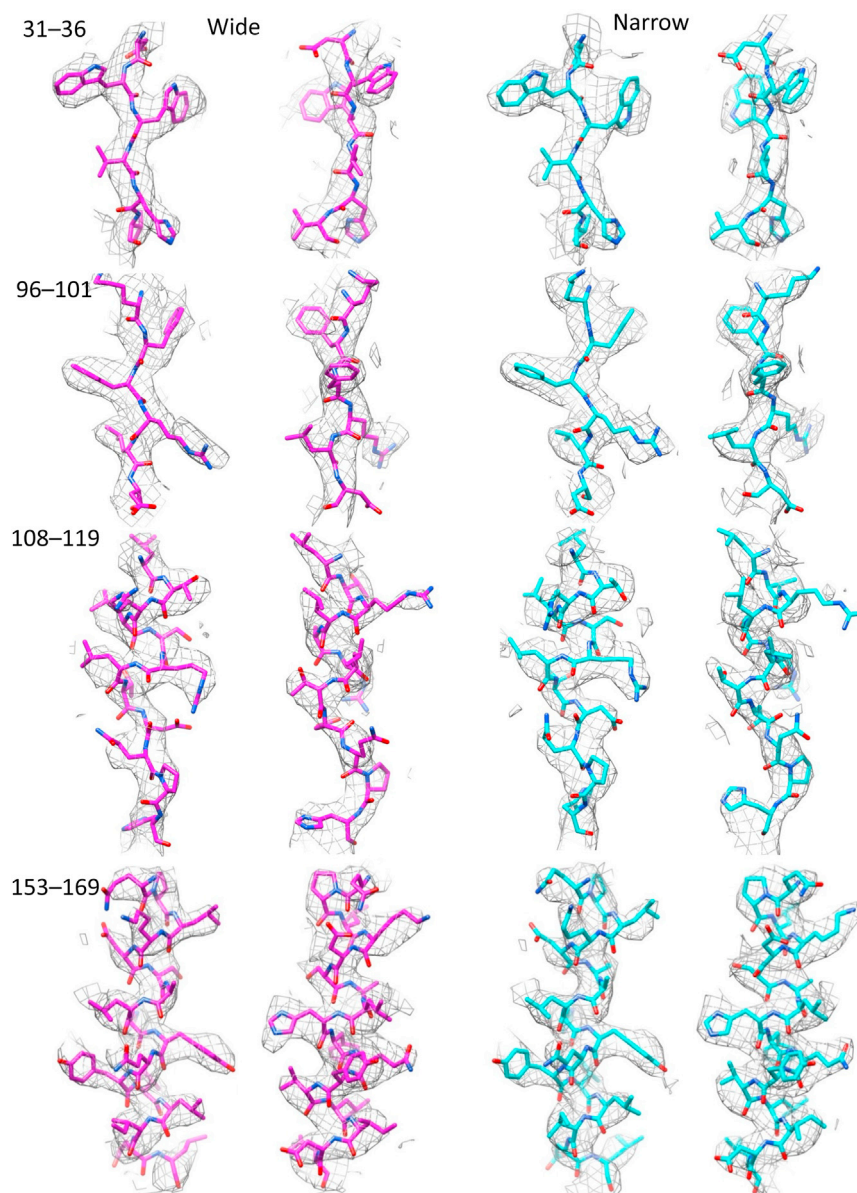
Contacts between Subunits of CP in BSMV

The CP in the narrow virion makes two lateral inter-subunit salt bridges compared with no inter-subunit salt bridges for the wide structure (Asp44-Arg69, Glu125-Arg128) (Figure 6 top, Figures 7A and 7B). In the wide virion, Arg69 makes a contact with Asn40 instead of Asp44, and Arg128 points toward the RNA instead of Glu125. All four residues of these two ion pairs are conserved in Poa semilatent virus (PSLV) (Solovyev et al., 1996) but only the Glu125-Arg128 residues are conserved in the other more distantly related viruses LRSV, peanut clump virus (PCV), and Indian peanut clump virus (IPCV) (Adams et al., 2011) (Figure S5). The density for the side chain of Glu125 in the wide structure is missing but the density for the Arg128 side chain in both the wide and narrow structure is complete. The density for the side chain of Glu125 in the narrow structure positions is close to Arg128, and it is possible that the side chain of Glu125 could occupy the same conformation as that seen in the wide structure, which means that Arg128 contacts the

Figure 4. Selected Regions of chBSMV Wide and Narrow Maps with Their Fitted Atomic Models

The wide coordinates are shown as magenta and the narrow coordinates as cyan. Each region is shown from two views, with the second view rotated by 90° from the first.

The absence of these axial contacts between CPs makes BSMV different from TMV, CGMMV, and HLSV, which have two axial salt bridge contacts. Even between these more closely related viruses, the residues involved in the axial salt bridge contacts vary between them (TMV Glu50-Arg134 and Glu95-Arg112; CGMMV Arg122-Asp42 and Lys134-Asp57; RMV Arg122-Asp42; HLSV Arg45-Asp126 and Asp116-Arg92 [Adams et al., 2011]). This makes it difficult to predict if any of the hordeiviruses closely related to BSMV would have axial salt bridges.

RNA Binding Site

The RNA is located at a radius of 50 Å and 53 Å from the center of the virion in narrow and wide virions, respectively. Arg122 contacts the RNA in both BSMV structures and is equivalent to Arg92 in TMV. This is the only strong axial contact in the BSMV virions. There is a small difference in the way Arg122 interacts with RNA between the narrow and wide structures. In the wide virion, Arg122 has a weak contact to the phosphate backbone of nucleotide 2 and a stronger contact to the sugar ring of nucleotide 3, and this contact may be stabilized in addition by Arg128 and Glu125 (Figure 9A, upper panels). In the narrow virion, Arg122 is located closer to phosphate backbone of nucleotide 2 than the sugar ring from nucleotide 3 (Figure 9A, bottom panels). In the narrow conformation, Arg128 is making a potential salt bridge to Glu125 and therefore does not interact with the RNA (Figure 7B and Figure 9A, bottom panels). The strong interaction between Arg122 and RNA may explain the large upward tilt of the inner part of the BSMV CP (Figure 5). BSMV does not have the equivalent of Arg90 from TMV that in combination with Arg92 sandwiches the phosphate backbone of RNA in TMV (seen only in cryo-EM [Clare and Orlova, 2010; Sachse et al., 2007]). BSMV also does not contain residues equivalent to Lys112 and Arg122 in CGMMV or Lys123 in HLSV that have been shown to interact with the phosphate backbone of the RNA (Figure S5). Arg57 (TMV: Arg41) is conserved in rod-like viruses and has been shown for CGMMV to interact with RNA. However, Arg57 does not contact the RNA in BSMV.

chBSMV-IY/GG-infected tissues, while virions were detected in chBSMV-infected plants. Also, clear differences in the absorption spectra of the wtBSMV samples, compared with preparations obtained for the mutants, indicated that the mutants were unable to form stable virions. This was also confirmed by EM, as the sap from infected plants revealed that virions were present only in chBSMV-infected plants (Figure 8). These results indicate that the inter-subunit lateral contact made by the insertion loop is essential for formation and/or maintaining the structure of BSMV visions.

BSMV virions have only one potential axial contact between CP subunits (Tyr63-Arg103) but the density for this contact is not very strong. Tyr63 is conserved only in BSMV and PSLV and Arg103 is not conserved in any of the viruses. The increased axial subunit distance by ∼ 6 Å may explain the lack of axial contacts/salt bridges between CP in BSMV compared with TMV.
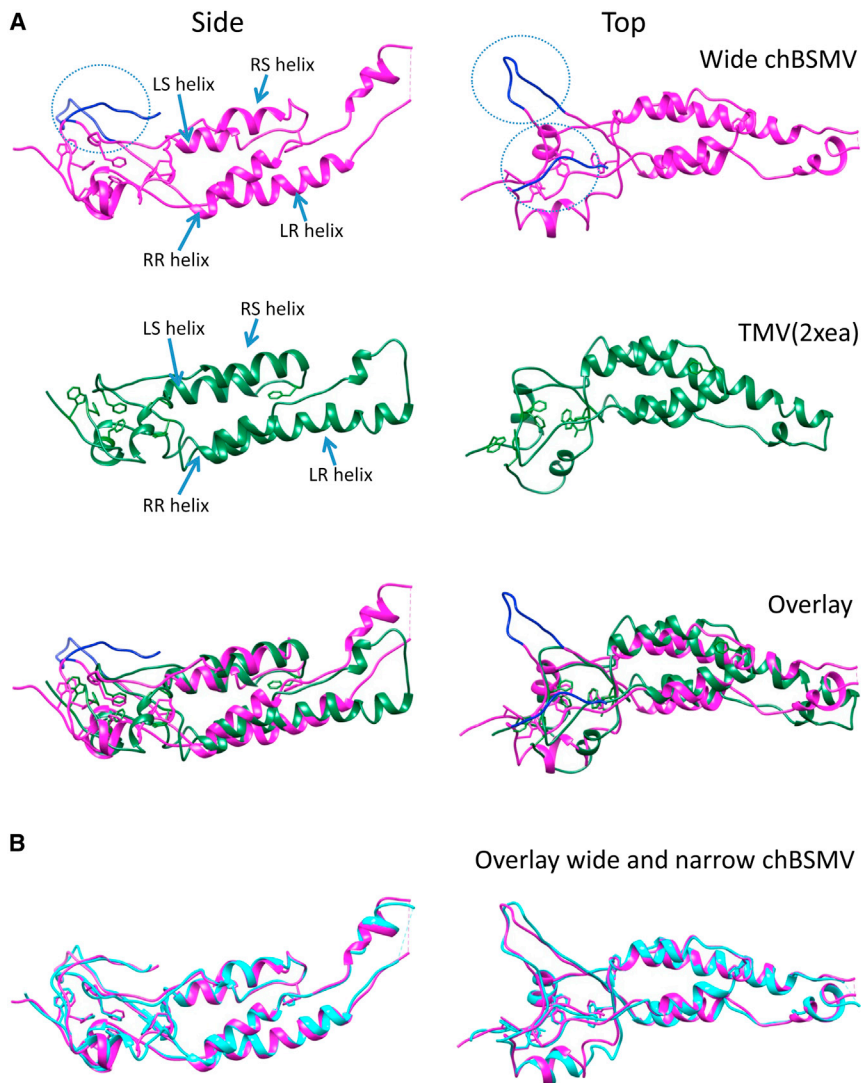
A

Figure 5. Comparison of chBSMV and TMV
(A) Atomic models for wide chBSMV (magenta) and TMV (green, PDB: 2xea). The structures are shown from the top and side and their overlay from the top and side. The side chains of the conserved residues in the hydrophobic core are displayed with all other atoms shown as C-α (BSMVaa = 14, 33, 51, 79, 98, 182, 188, 190 and TMVaa = 2, 17, 35, 62, 70, 144, 150, 152). The insertions in the BSMV structure when compared with TMV are shown in blue and highlighted with dashed circles (aa 3–10 and aa 84–94).
(B) Overlay of the coordinates for wide (magenta) and narrow (cyan) chBSMV structures. The same conserved hydrophobic residues from part (A) are shown as side chains. The inner loops of both wide and narrow BSMV CP proteins are missing in the cryo-EM density (missing residues from the inner loops of BSMV include 132–146 in wide and 132–147 in narrow).

Tyr164 forms, previously unobserved in rod-shaped viruses, a pi-pi/base stacking interaction with the nitrogen base of nucleotide 2 of the RNA (Figure 9B, left column). Tyr in this position is conserved in the other hordeiviruses and in the IPCV. Tyr-RNA base stacking has also been observed in bacteriophage CPs (Johansson et al., 1997; Rumnieks and Tars, 2014). On the opposite side of the helix to Tyr164 is Tyr162 (Figure 9B, left column), which is positioned in a hydrophobic pocket created by Val60, phe51, Leu46, Ile49, Leu111, and Leu166 within the same subunit. The residue in the equivalent position to Tyr162 is either a Tyr in PCV or phenylalanine in PLSV, LRSV, and PCV and an isoleucine in TMV.

Tyr162 also makes a potential hydrogen bond to Arg113 of the adjacent subunit (Arg113 conserved only in PLSV, LRSV, and PCV). Both of these interactions help to stabilize the RNA binding region of BSMV. Residues that form the hydrophobic pocket around Tyr162 are well conserved. Val60 is conserved in the most closely related viruses and is also found in TMV and RMV. Phe51 is present in the most closely related viruses apart from LRSV and Leu46 is conserved in closely related viruses. Leu111 is conserved in most rod-shaped viruses and Leu166 is present in all BSMV-like viruses but is substituted for Ile in the TMV-like viruses (Figure S5). Ile49 and Leu114 are not absolutely conserved but are replaced by similar small hydrophobic side chains.

There are also a number of hydrophilic/charged residues located around the RNA. From the subunit that contributes Arg122 (from below the RNA) there are also Asn50, Ser55, Ser56, and Asn121 close to the RNA. The subunit that contacts RNA via Asp157, Leu160, His161, and Tyr164 also contributes Gln117, Lys156, Gln153, and Gln163. All of these residues must help create a hydrophilic environment for the RNA while it

BSMV has the same helix extension as TMV in the RR helix, proposed to help stabilize the protein RNA interaction (Clare and Orlova, 2010; Sachse et al., 2007) but, since it does not have Arg90, it does not make the RNA-arginine sandwich. Asp157 is located under the RNA phosphate backbone (closest to phosphate of nucleotide 2) and has close contact with the nitrogen base of nucleotide 3 via the main chain between it and Ser158 (Figure 9B, right column). Asp157 is equivalent to the Asp116 from TMV and is conserved in all rod-shaped viruses and has the same contact as that observed in TMV. Leu160 makes a hydrophobic contact to the nitrogen base of nucleotide 1 in BSMV (Figure 9B, middle column). A small hydrophobic residue is seen at this position in most of the helical viruses and seems to be a conserved contact. His161, on the opposite side of the helix to Leu160, interacts with the nitrogen base of nucleotide 3 in BSMV (Figure 9B, middle column). Histidine is also seen at this position in LRSV and IPCV-L but not in PSLV, IPCV-D, and PCV, where it is replaced by a serine or asparagine residue. The equivalent residue in the sequence to His161 is an alanine in the tobamoviruses.
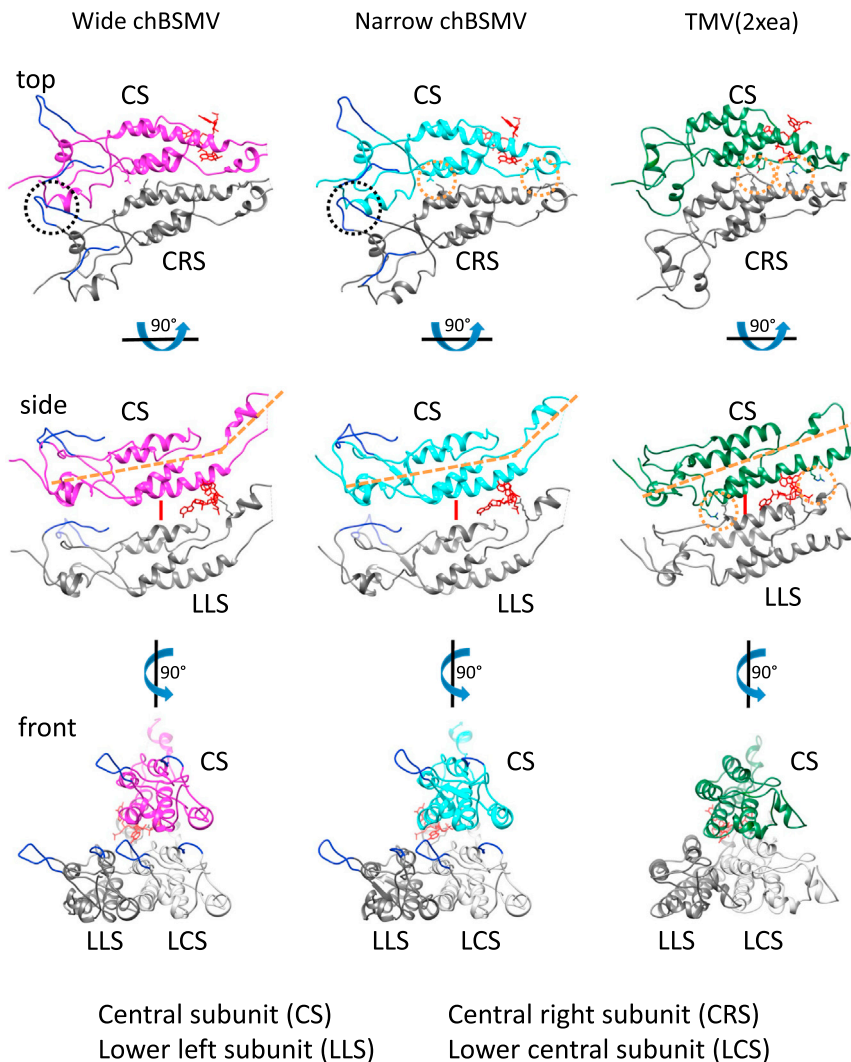
Figure 6. Comparison of chBSMV and TMV CP Packing

Atomic models for wide chBSMV (magenta, left column), narrow chBSMV (cyan, central column), and TMV (green, right column). The structures are shown from the top, the side, and the front (axes of rotation are displayed). Adjacent lateral and axial subunits are shown in the different views labeled according to their local position in the helix of the capsid (see labels at the bottom of the figure). The insertions in BSMV, when compared with TMV, are shown in blue (aa 3–10 and aa 84–94) and the RNA for the CS subunits is shown in red. Gold dashed circles highlight the location of the inter-subunit salt bridges. Specifically, in a narrow BSMV structure, the potential lateral salt bridges formed between residues Arg69–Asp44 (near the center of subunit) and Glu128–Arg128 (close to the inner channel). In TMV, the lateral salt bridges formed by residues Asp88–Arg122 and Arg113–Asp115 (closer to the inner loop) and the axial salt bridges formed by Arg134–Glu50 (close to the outer surface) and Arg112–Glu95 (close to the inner surface, only in fiber diffraction structure). The black dashed circles mark the lateral contact between the insertion loop of BSMV (aa84–94) with its neighboring subunit. The major axes of the BSMV and TMV subunits are marked on the side views using gold dashed lines. The blue lines drawn on the side views are the same length and highlight the increase in axial distance between the BSMV subunits compared with TMV.

Central subunit (CS)   Central right subunit (CRS)
Lower left subunit (LLS)   Lower central subunit (LCS)

is encapsidated. A number of these residues are conserved in the BSMV-like viruses: Asn50, Ser55, Ser56, Gln117, and Gln153, while the others have conservative amino acid substitutions such as Lys156 to Arg. One residue is conserved with the TMV-like viruses and that is Asn121 (Asn91 in TMV). Only Gln163 is not conserved.

Caspar Carboxylates

Casper carboxylates (CC) are clusters of negatively charged residues that act as metastable switches in TMV (Caspar, 1963; Namba and Stubbs, 1986; Wang et al., 1998). When the carboxylate group of these residues are pronated or bound to calcium, and therefore not charged, the switch is in the off position. However, when the carboxylate groups are de-protonated or calcium is removed, they repel each other and therefore promote disassembly of TMV. TMV has two CC clusters formed at high radius by Glu50 and Asp77 and at low radius by glu95, 97, 106, and 109. There is a potential high-radius CC cluster observed in BSMV between residues Glu37–Asp70 (C-α carbon distance 8.7 Å and 9.6 Å, in the wide and narrow structures, respectively) and Glu37–Asp74 (C-α carbon distance 12.6 Å in both the narrow

and wide structures) (Figure 10), similar to that in the TMV-like viruses. Glu37 is either a Glu or Asp, while Asp70 is conserved in PLSV, LRSV, PCV, and IPCV-L/D but Asp74 is only in BSMV, PLSV, and IPCV-D. These potential CC residues are very close to the Asp44–Arg69 salt bridge and could disrupt that connection. In the narrow structure, Glu37 is farther away from Asp70 and Asp74 (C-α carbon distance 7.2 Å for both Glu37-Asp70 and Asp74, with C-α carbon distance of 9.6 Å for Glu37-Asp70 and 12.6 Å for Glu37-Asp74). However, there is no density for the side chain of Glu37 in either wide or narrow virions, making it difficult to localize the accurate position of the Glu37 side chain. The lack of density for negatively charged residues is a common feature of high-resolution cryo-EM maps, as they are suggested to be the most radiation sensitive (Sachse et al., 2007).

The low-radius CC observed in TMV (RMV, CGMMV, HLSV Glu95, Glu97, Glu98, Glu99, Glu106, Glu46, and Glu130) is not, however, conserved in BSMV or in the more closely related viruses; the only residue that is conserved is Glu125 (TMV Glu95), which is involved in an inter-subunit salt bridge with Arg128 in the narrow virion. Arg128 is conserved in *Hordeivirus* and one would expect that it could make the same contact in these viruses. This suggests that the low-radius CC cluster is not present in BSMV and its related viruses, implying that the uncoating process in rod-shaped viruses may not be conserved.
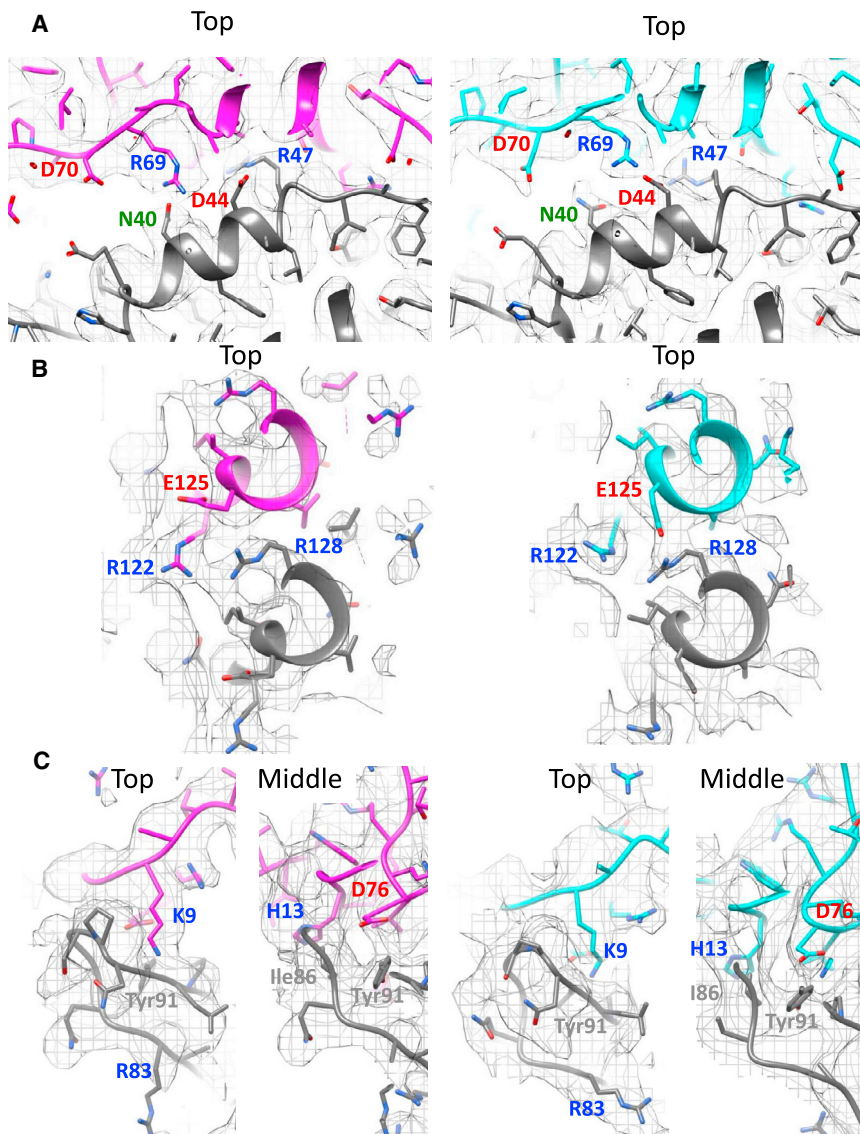
Figure 7. Lateral Contacts between chBSMV CP

(A) The potential salt bridge formed between Arg69 and Asp44 in the narrow chBSMV structure (cyan and dark gray coordinates) compared with the wide (magenta and dark gray coordinates) shown from the top. In the wide structure, Arg69 makes a contact with Asn40 instead of Asp44.

(B) A second potential salt bridge is formed between Arg128 and Glu125 in the narrow structure (cyan and dark gray) compared with the wide structure (magenta and dark gray) shown from the top.

(C) Contact between the insertion loop 84–94 with the neighboring subunit shown from the top and middle of the contact for the wide (magenta and dark gray) and narrow (cyan and dark gray). Asp76 makes a contact with the ring of Tyr91, Lys 9 makes a contact with the main chain of Tyr91, and Ile86 seems to make a contact with His13. The cryo-EM density is shown as gray mesh in all panels.

17 CP subunits (Butler, 1999). Mandelkow et al. (1976) also observed that at low pH (5.5), TMV forms two types of helices, one with 16.3 and the other with 17.3 subunits per turn, with both helices having the same pitch of 22.88 Å. However, the structures of these two complexes were not determined because of problems with obtaining well-oriented sample gels.

For both 4.1 Å chBSMV structures, we were able to trace the polypeptide chain, and our results confirmed that CP of *Tobamovirus* and *Hordeivirus* genera have similar folds, with a number of key conserved residues located in similar positions in both. Furthermore, both BSMV and TMV CP subunits contact encapsidated RNA by conserved residues, Arg122 and Asp157 in BSMV corresponding to Arg92 and Asp116 in TMV. We also found a new type of RNA contact in rod-shaped viruses, as Tyr164 forms a pi-pi/base stacking interaction with RNA (Figure 9). Tyr at this position is conserved in the other hordeiviruses and IPCV. The Tyr-RNA interaction observed in the BSMV virions has also been detected in bacteriophage CPs (Rumnieks and Tars, 2014). Tyr-base interaction would work for all bases allowing promiscuity in RNA binding, which explains the ability of the BSMV CPs to bind to different RNAs in a sequence-independent manner and may reflect a characteristic feature of viruses with multipartite genomes.

The variance in diameter between the wide and narrow virions correlates with differences in specific contacts between the CP. In particular, the CP subunits in the narrow virions have two lateral salt bridges (residues Asp44-Arg69 and Glu125-Arg128) similar to TMV and the other tobamoviruses (Tewary et al., 2011), which are not observed in the wide virions. The presence of the lateral salt bridges in the narrow form suggests that the narrow BSMV structure could be more stable than the wide

DISCUSSION

We used cryo-EM and single-particle analysis to determine the structure of rod-shaped plant virus BSMV at near-atomic resolution, which has allowed us to build an atomic model of the BSMV CP. Our study has shown that BSMV forms two different virions, the narrow and wide, which have diameters of 216 Å and 224 Å, respectively. The formation of these virions is not dependent on the type of RNA, since both the wt- and chBSMV have narrow and wide virions. The difference in the virion diameter is associated with a change in the number of CP per turn, as the narrow virion has one CP unit less per turn compared with the wide virion. This is the first time that variations in packaging of the rod-like helical plant viruses, when encapsidated RNA, have been observed. So far, all studied species of *Tobamovirus* have had the same helical symmetry when encapsidated RNA (16.3 subunits per turn). However, without RNA, the TMV CP forms double-layered cyclical disks, in which each layer contains
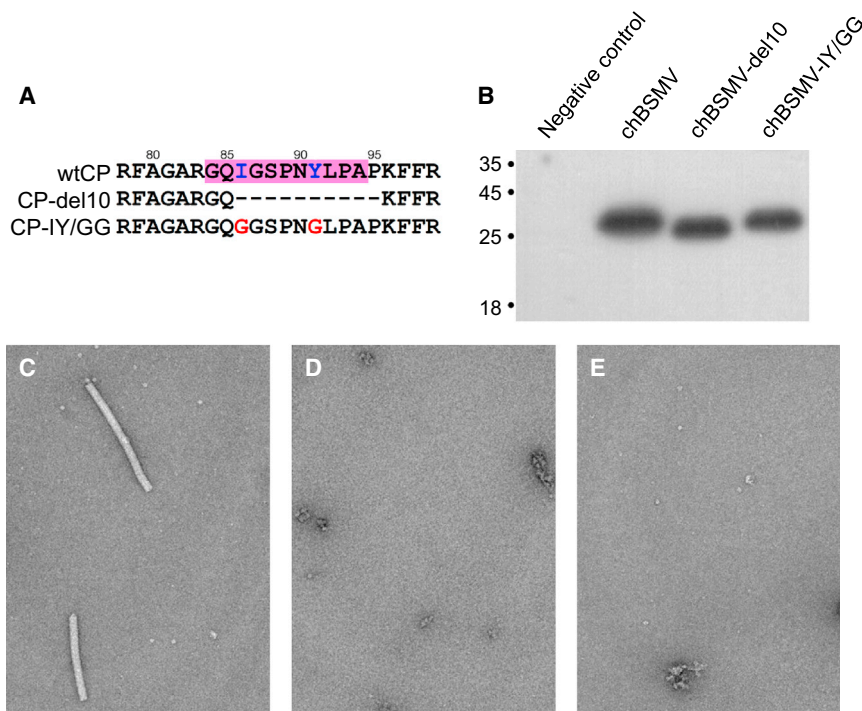
Figure 8. Analysis of BSMV CP Mutants

(A) Mutations del10 and IY/GG in the BSMV CP. The insertion loop is marked with pink in the wtBSMV CP sequence. Deleted residues are represented by dashes and mutated residues are shown in magenta.
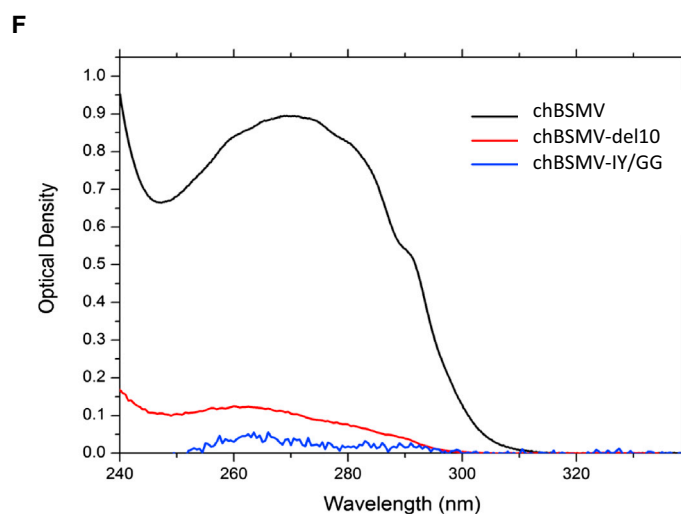
(B) Western blot analysis of virus accumulation in systemically infected leaves of plants inoculated with chBSMV, chBSMV-del10, and chBSMV-IY/GG. The virus CP was detected with a BSMV-specific antiserum. "Negative control" was a sample from a non-inoculated plant. Protein molecular weight markers are shown on the right.

(C) Image of negatively stained sample from plants inoculated with chBSMV. The image shows the presence of fully assembled chBSMV virions.

(D) Image of negatively stained sample from plants inoculated with mutant chBSMV-del10 (deleted loop 85–96 aa).

(E) Image of negatively stained sample from plants inoculated with the chBSMV-IY/GG mutant. Samples in (D) and (E) did not show any virions.

(F) Absorption spectra of chBSMV virions that coincide with spectra of the wtBSMV (Makarov et al., 2013), chBSMV-del10, and chBSMV-IY/GG.

environment. However, further studies are required to demonstrate whether the structural transition between the two BSMV forms can occur and to determine what factors could induce such a transition. Low-radius CC known to be essential for disassembly of TMV virions are absent in both BSMV structures, suggesting that BSMV could have a different uncoating mechanism, which might be envisaged to involve a transition from the narrow to the wide virion form.

In both wide and narrow BSMV virions, the CP forms an inter-subunit contact near the surface of the virion via the interacting loop (insertion loop 84–94 aa) that protrudes from the hydrophobic core of one CP toward the adjacent lateral CP. This inter-subunit interaction is not observed in TMV as this interacting loop

one. Particularly as BSMV does not have any clear axial contacts between CP, unlike the tobamoviruses, so predominantly the lateral contacts are holding the CP together, and apparently, these lateral contacts are strengthened by the interaction at the outer surface of the capsid formed by the insertion loop of BSMV (aa84-94). The RNA chain also contributes to the axial contact between the CPs.

Furthermore, Arg122 in BSMV interacts with the RNA differently in the wide and narrow virions, with the wide virion potentially having a weaker interaction via Arg122 to RNA. It is possible that co-existence of both BSMV forms may have an adaptive function for the virus: a population of virus particles can comprise both uncoating-ready wide virions and stable narrow virions that are destined to retain their structural integrity in a non-favorable

is absent in the CP of tobamoviruses. Furthermore, this newly found lateral contact between CPs is essential for formation and maintaining the structure of BSMV virions, as deletion or mutation of this loop prevents the assembly of stable BSMV virions in plants. The lateral inter-subunit contact formed by the interacting loop is reminiscent of the interaction between CPs of the papaya mosaic virus (PapMV), a flexible filamentous virus (genus *Potexvirus*, family Alphaflexiviridae), which has a CP with a long N terminus (26 aa) that contacts the neighboring CP (Yang et al., 2012). Although BSMV and PapMV CP have unrelated folds, it is tempting to speculate that there may be a common type of inter-subunit interaction in both the rod-shaped and flexible virions. Verification of this hypothesis would require high-resolution structures of a number of filamentous viruses.
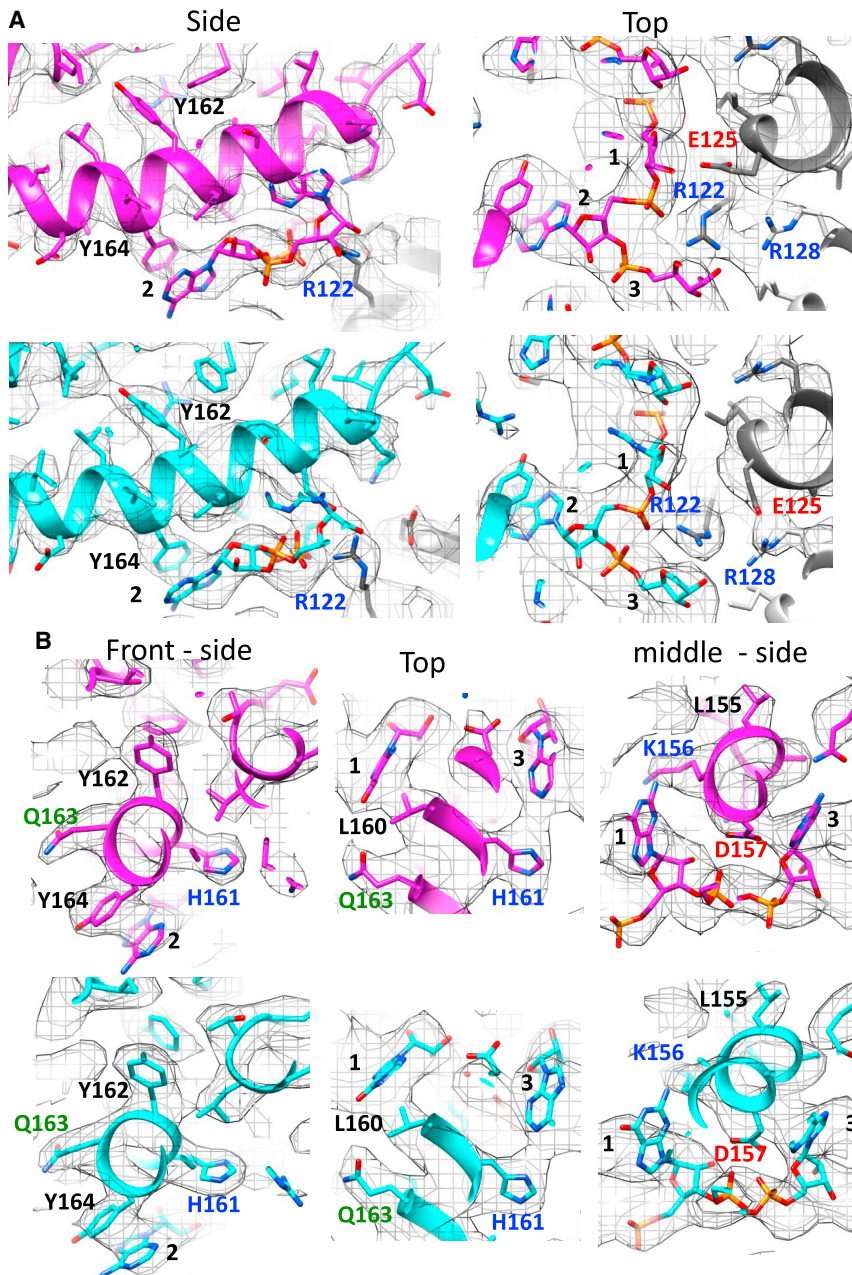
A Side

B Front - side, Top, middle - side

(A) Arg122, from the subunit below (dark gray), makes its strongest contact to the sugar ring of nucleotide 3 in the wide (magenta) and to the phosphate backbone of nucleotide 2 in the narrow structure (cyan). This is shown from the side and the top. In the view from the top, Arg128 from the neighboring subunit is also shown.

(B) Other residues involved in RNA binding are shown from the front side, top and middle side for the wide (magenta) and narrow structures (cyan) including residues Tyr164, His161, Leu160, and Asp157.

novel principles of helical structure organization described here for BSMV are widespread among viruses of this type. It is necessary to add that recently, rod-shaped viruses have become a subject of special interest for their application as biotemplates in the production of novel inorganic materials (Love et al., 2014), in particular metal nanoparticles and nano-wires (Aljabali et al., 2010, 2011; Wnek et al., 2013). Our new BSMV structure reported here represent a foundation for similar applications. We believe that, in addition to new insights into structural organization of helical plant viruses, this work will also stimulate further mutational analyses to control and alter the virion structure of BSMV for its usage as a biotemplate.

EXPERIMENTAL PROCEDURES

Virions Isolation and Construction of Recombinant Clones

The isolation of BSMV virions has been carried out as previously described (Makarov et al., 2013). Specific details of the virus isolation are in the Supplemental Information.

Chimeric construct TMV:BSMV-CP was based on the vector TMV-M2e-ala (Petukhova et al., 2013) modified to introduce an XhoI site between the 30-kDa movement protein gene and the *cp* gene (Figure 1) and an XbaI site just upstream of the TMV genome 3′-untranslated region. The BSMV *cp* gene was amplified with a pair of specific primers and cloned as an XhoI/XbaI fragment into the modified TMV-M2e-ala. The resulting TMV:BSMV-CP construct represented a binary vector pBin19 containing the recombinant virus genome under the control of the *Arabidopsis thaliana* actin-2 promoter and the nopaline synthase transcriptional terminator. An *Agrobacterium tumefaciens* (strain GV3101) culture containing the chimeric TMV:BSMV-CP construct was used for infiltration of *Nicotiana benthamiana* leaves to initiate virus systemic infection. TMV:BSMV-CP chimeric complex (chBSMV) was isolated from systemically infected leaves as described for BSMV (see Supplemental Information).

EM

The BSMV samples were diluted to a final concentration of 3 mg/ml in 50 mM Tris–HCl (pH 7.4), 50 mM KCl, 10 mM MgCl₂. 3.5 µl of the BSMV was applied to

The alignment of CP sequences encoded by six genera comprising the family Virgaviridae reveals that all viruses except those of the genus *Tobamovirus* have the sequence, potentially forming a BSMV-like interacting loop (Figures S5 and S6). Since tobamoviruses represent an apparent exception among rod-shaped viruses with closely related CPs (Dolja et al., 1991), one can presume that the interacting loop has been lost in the evolutionary history of the genus *Tobamovirus* and the tobamovirus CP has evolved a different mechanism for stabilization of inter-subunit interaction using axial salt bridges.

The data obtained for BSMV have increased the knowledge on the structure of helical plant viruses previously limited to the structures of tobamoviruses. Future high-resolution studies of other rod-shaped and filamentous viruses will elucidate whether
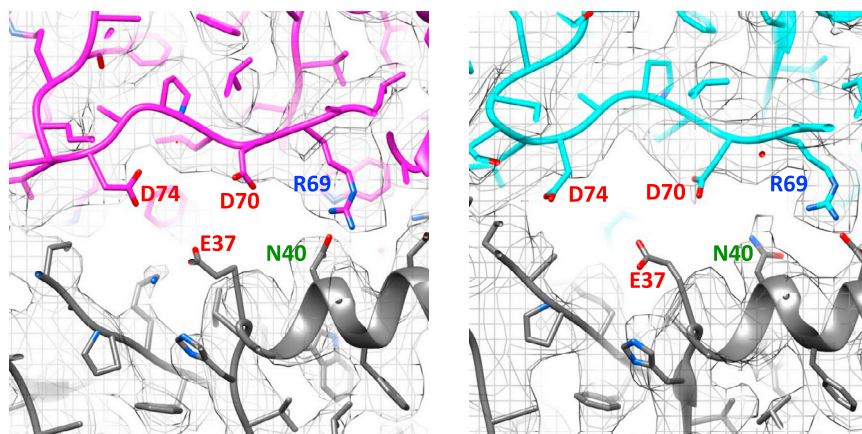
Figure 10. Potential Casper Carboxylates at High Radius

Casper carboxylates at high radius, shown from the top, for both the wide (magenta and dark gray) and narrow (cyan and dark gray) structures. CC clusters are important for the uncoating of TMV via pH-induced charge repulsion upon entering the host plant.

either C-flat grids (r2/2, Protochips) or homemade continuous carbon films, which had been rendered hydrophilic by glow discharge in air. The grids were then blotted and frozen in liquid nitrogen cooled liquid ethane. Low-dose images (20–25 e⁻/Å²) were manually recorded on a Tecnai Polara EM (FEI) operated at 300 keV, using a Gatan Ultrascan 4,000 4k × 4k CCD camera with an ultra-sensitive phosphor scintillator (Gatan) with a calibrated magnification of 150,000×, giving 1 Å/pixel on the images. A defocus range between 0.7 and 3.0 μm underfocus was used during data collection. Correction for the effects of the contrast transfer function is described in Supplemental Information.

Reconstruction Procedure

Assessment of helical parameters of rod-like virions was carried out on contrast transfer function-corrected images of negatively stained samples and is described in the Supplemental Information.

Statistical analysis on images after the alignment showed eigen images that suggested that both the wtBSMV and chBSMV viruses had variations in width (Figure S1). The eigen images corresponding to the size variation in the two datasets were then used to separate each dataset initially into three classes: narrow, intermediate, and wide. All three classes were reconstructed using the same symmetry parameters, and it was clear that only the wide class had 22.2 subunits per ring with five rings per period. The symmetry parameters were screened for both the narrow and intermediate classes in both datasets, and the narrow class gave the best result using 21.2 subunits per turn with five turns and the intermediate would not refine. Upon closer inspection, it looked like the intermediate set were just a mix of wide and narrow virions. The separation and reconstruction of the wide and narrow sets were then refined and this is explained in the Supplemental Information.

Homology Modeling and Flexible Fitting

A homology model of BSMV CP was generated using I-TASSER (Roy et al., 2010). It was fitted into the sharpened wide and narrow (Figure 3; Figure S3) chBSMV reconstructions using Flex-EM (Topf et al., 2008). The initial approximate fitting of the homology models was manually refined using Coot (0.7.2) (Emsley et al., 2010) and then computationally refined with PHENIX (Adams et al., 2009). After PHENIX refinement, errors in the coordinates were fixed with Coot. This process was iterated until the optimal fit between the coordinates and the density was achieved and when the geometry and Ramachandran parameters were optimized (Figures S9 and S10). The coordinates were then checked using MolProbity (Chen et al., 2010) with the overall quality score calculated at 2.76 for both the wide and the narrow structures. Visualization of maps and fitting was done using Chimera (Goddard et al., 2007).

ACCESSION NUMBERS

The EM density maps have been deposited in the EMDB (http://www.ebi.ac.uk/pdbe/) with accession codes EMD-3073 and EMD-3077 for chBSMV and wtBSMV wide virions and EMD-3074 and EMD-3078 for chBSMV and wtBSMV narrow virions and the coordinates were deposited in the PDB with accession codes PDB: 5a79 for the wide structure and PDB: 5a7a for the narrow structure.

SUPPLEMENTAL INFORMATION

Supplemental Information includes Supplemental Experimental Procedures, ten figures, and one table and can be found with this article online at http://dx.doi.org/10.1016/j.str.2015.06.028.

AUTHOR CONTRIBUTIONS

O.S.S., V.M., D.C., A.G.S., and E.V.O. designed the experiments. E.S., V.M., and A.G.S. performed biochemistry and mutagenesis. V.M. performed experiments with absorption spectra. D.C., O.S.S., and E.V.O. trained E.P. D.C. and E.P. performed EM and image analysis. D.C., P.E., and E.V.O. analyzed the EM data. D.C. performed modeling and fitting to interpret the data. D.C., A.G.S., and E.V.O. wrote the article. A.G.S. and E.V.O. supervised the work.

ACKNOWLEDGMENTS

REFERENCES

Adams, P.D., Mustyakimov, M., Afonine, P.V., and Langan, P. (2009). Generalized X-ray and neutron crystallographic analysis: more accurate and complete structures for biological macromolecules. Acta Crystallogr. D Biol. Crystallogr. *65*, 567–573.

Adams, M.J., Heinze, C., Jackson, A.O., Kreuze, J.F., Macfarlane, S.A., and Torrance, L. (2011). Family Virgaviridae. In Virus Taxonomy: Ninth Report of the International Committee on Taxonomy of Viruses, A.M.Q. King, M.J. Adams, E.B. Carstens, and E.J. Lefkowitz, eds. (Elsevier), pp. 1139–1162.

Aljabali, A.A.A., Barclay, J.E., Lomonossoff, G.P., and Evans, D.J. (2010). Virus templated metallic nanoparticles. Nanoscale *2*, 2596–2600.

Aljabali, A.A.A., Shah, S.N., Evans-Gowing, R., Lomonossoff, G.P., and Evans, D.J. (2011). Chemically-coupled-peptide-promoted virus nanoparticle templated mineralization. Integr. Biol. (Camb.) *3*, 119–125.

Atabekov, I.G., and Novikov, V.K. (1966). The properties of barley mosaic virus nucleoprotein and its structural components. Biokhimiia *31*, 157–166, (in Russian).

Atabekov, J.G., and Novikov, V.K. (1971). Barley Stripe Mosaic Virus. Descriptions of Plant Viruses (Commonwealth Mycological Institute and Association of Applied Biologists), 4 p. no. 68.

Atabekov, J.G., Novikov, V.K., Kiselev, N.A., Kaftanova, A.S., and Egorov, A.M. (1968). Stable intermediate aggregates formed by the polymerization of barley stripe mosaic virus protein. Virology 36, 620–638.

Bhyravbhatla, B., Watowich, S.J., and Caspar, D.L. (1998). Refined atomic model of the four-layer aggregate of the tobacco mosaic virus coat protein at 2.4-A resolution. Biophys. J. 74, 604–615.

Butler, P.J. (1999). Self-assembly of tobacco mosaic virus: the role of an intermediate aggregate in generating both specificity and speed. Philos. Trans. R. Soc. Lond. B Biol. Sci. 354, 537–550.

Caspar, D.L. (1963). Assembly and stability of the tobacco mosaic virus particle. Adv. Protein Chem. 18, 37–121.

Chen, V.B., Arendall, W.B., 3rd, Headd, J.J., Keedy, D.A., Immormino, R.M., Kapral, G.J., Murray, L.W., Richardson, J.S., and Richardson, D.C. (2010). MolProbity: all-atom structure validation for macromolecular crystallography. Acta Crystallogr. D Biol. Crystallogr. 66, 12–21.

Clare, D.K., and Orlova, E.V. (2010). 4.6A Cryo-EM reconstruction of tobacco mosaic virus from images recorded at 300 keV on a 4k × 4k CCD camera. J. Struct. Biol. 171, 303–308.

Dolja, V.V., Boyko, V.P., Agranovsky, A.A., and Koonin, E.V. (1991). Phylogeny of capsid proteins of rod-shaped and filamentous RNA plant viruses: two families with distinct patterns of sequence and probably structure conservation. Virology 184, 79–86.

Emsley, P., Lohkamp, B., Scott, W.G., and Cowtan, K. (2010). Features and development of Coot. Acta Crystallogr. D Biol. Crystallogr. 66, 486–501.

Finch, J.T. (1965). Preliminary X-ray diffraction studies on tobacco rattle and barley stripe mosaic viruses. J. Mol. Biol. 12, 612–619.

Ge, P., and Zhou, Z.H. (2011). Hydrogen-bonding networks and RNA bases revealed by cryo electron microscopy suggest a triggering mechanism for calcium switches. Proc. Natl. Acad. Sci. USA 108, 9637–9642.

Goddard, T.D., Huang, C.C., and Ferrin, T.E. (2007). Visualizing density maps with UCSF Chimera. J. Struct. Biol. 157, 281–287.

Jackson, A., and Lane, L. (1981). Hordeiviruses. In Handbook of Plant Virus Infections and Comparative Diagnosis, E. Kurstak, ed. (Elsevier), pp. 565–625.

Jackson, A., Hunter, B., and Gustafson, G. (1989). Hordeivirus relationships and genome organization. Annu. Rev. Phytopathol. 27, 95.

Jackson, A.O., Lim, H.-S., Bragg, J., Ganesan, U., and Lee, M.Y. (2009). Hordeivirus replication, movement, and pathogenesis. Annu. Rev. Phytopathol. 47, 385–422.

Johansson, H.E., Liljas, L., and Uhlenbeck, O.C. (1997). RNA recognition by the MS2 phage coat protein. Semin. Virol. 8, 176–185.

Kendall, A., Williams, D., Bian, W., Stewart, P.L., and Stubbs, G. (2013). Barley stripe mosaic virus: structure and relationship to the tobamoviruses. Virology 443, 265–270.

Kiselev, N.A., Atabekov, I.G., Kaftanova, A.S., and Novikov, V.K. (1966). Study of virus protein repolymerization and resynthesis of rod-like viruses. Biokhimiia 31, 670–678, (in Russian).

Kiselev, N.A., DeRosier, D.J., and Atabekov, J.G. (1969). A double-helical structure found on the re-aggregation of the protein of barley stripe mosaic virus. J. Mol. Biol. 39, 673–674.

Love, A.J., Makarov, V., Yaminsky, I., Kalinina, N.O., and Taliansky, M.E. (2014). The use of tobacco mosaic virus and cowpea mosaic virus for the production of novel metal nanomaterials. Virology 449, 133–139.

Makarov, V.V., Skurat, E.V., Semenyuk, P.I., Abashkin, D.A., Kalinina, N.O., Arutyunyan, A.M., Solovyev, A.G., and Dobrov, E.N. (2013). Structural lability of barley stripe mosaic virus virions. PLoS One 8, e60942.

Mandelkow, E., Holmes, K.C., and Gallwitz, U. (1976). A new helical aggregate of tobacco mosaic virus protein. J. Mol. Biol. 102, 265–285.

McKinney, H.H. (1951). A seed-borne virus causing false stripe symptoms in barley. Phytophotology 41, 563–564.

Namba, K., and Stubbs, G. (1986). Structure of tobacco mosaic virus at 3.6 A resolution: implications for assembly. Science 231, 1401–1406.

Namba, K., Pattanayek, R., and Stubbs, G. (1989). Visualization of protein-nucleic acid interactions in a virus. Refined structure of intact tobacco mosaic virus at 2.9 A resolution by X-ray fiber diffraction. J. Mol. Biol. 208, 307–325.

Orlova, E.V., and Saibil, H.R. (2010). Methods for three-dimensional reconstruction of heterogeneous assemblies. Methods Enzymol. 482, 321–341.

Pattanayek, R., and Stubbs, G. (1992). Structure of the U2 strain of tobacco mosaic virus refined at 3.5 A resolution using X-ray fiber diffraction. J. Mol. Biol. 228, 516–528.

Petukhova, N.V., Gasanova, T.V., Stepanova, L.A., Rusova, O.A., Potapchuk, M.V., Korotkov, A.V., Skurat, E.V., Tsybalova, L.M., Kiselev, O.I., Ivanov, P.A., et al. (2013). Immunogenicity and protective efficacy of candidate universal influenza A nanovaccines produced in plants by tobacco mosaic virus-based vectors. Curr. Pharm. Des. 19, 5587–5600.

Roy, A., Kucukural, A., and Zhang, Y. (2010). I-TASSER: a unified platform for automated protein structure and function prediction. Nat. Protoc. 5, 725–738.

Rumnieks, J., and Tars, K. (2014). Crystal structure of the bacteriophage Qbeta coat protein in complex with the RNA operator of the replicase gene. J. Mol. Biol. 426, 1039–1049.

Sachse, C., Chen, J.Z., Coureux, P.-D., Stroupe, M.E., Fandrich, M., and Grigorieff, N. (2007). High-resolution electron microscopy of helical specimens: a fresh look at tobacco mosaic virus. J. Mol. Biol. 371, 812–835.

Schon, A., and Mundry, K.W. (1984). Coordinated two-disk nucleation, growth and properties, of virus-like particles assembled from tobacco-mosaic-virus capsid protein with poly(A) or oligo(A) of different length. Eur. J. Biochem. 140, 119–127.

Solovyev, A.G., Savenkov, E.I., Agranovsky, A.A., and Morozov, S.Y. (1996). Comparisons of the genomic cis-elements and coding regions in RNA beta components of the hordeiviruses barley stripe mosaic virus, lychnis ringspot virus, and poa semilatent virus. Virology 219, 9–18.

Stubbs, G., Warren, S., and Holmes, K. (1977). Structure of RNA and RNA binding site in tobacco mosaic virus from 4-A map calculated from X-ray fibre diagrams. Nature 267, 216–221.

Tewary, S.K., Oda, T., Kendall, A., Bian, W., Stubbs, G., Wong, S.-M., and Swaminathan, K. (2011). Structure of hibiscus latent Singapore virus by fiber diffraction: a nonconserved his122 contributes to coat protein stability. J. Mol. Biol. 406, 516–526.

Topf, M., Lasker, K., Webb, B., Wolfson, H., Chiu, W., and Sali, A. (2008). Protein structure fitting and refinement guided by cryo-EM density. Structure 16, 295–307.

van Heel, M., Gowen, B., Matadeen, R., Orlova, E.V., Finn, R., Pape, T., Cohen, D., Stark, H., Schmidt, R., Schatz, M., et al. (2000). Single-particle electron cryo-microscopy: towards atomic resolution. Q. Rev. Biophys. 33, 307–369.

Veerisetty, V. (1978). Relationships among structural parameters of virions of helical symmetry. Virology 84, 523–529.

Wang, H., and Stubbs, G. (1993). Molecular dynamics in refinement against fiber diffraction data. Acta Crystallogr. A 49, 504–513.

Wang, H., and Stubbs, G. (1994). Structure determination of cucumber green mottle mosaic virus by X-ray fiber diffraction. Significance for the evolution of tobamoviruses. J. Mol. Biol. 239, 371–384.

Wang, H., Planchart, A., and Stubbs, G. (1998). Caspar carboxylates: the structural basis of tobamovirus disassembly. Biophys. J. 74, 633–638.

Wiese, M.V. (1987). Compendium of Wheat Diseases, Second Edition (American Phytopathological Society).

Wnek, M., Gorzny, M.L., Ward, M.B., Walti, C., Davies, A.G., Brydson, R., Evans, S.D., and Stockley, P.G. (2013). Fabrication and characterization of gold nano-wires templated on virus-like arrays of tobacco mosaic virus coat proteins. Nanotechnology 24, 025605.

Yang, S., Wang, T., Bohon, J., Gagne, M.-E.L., Bolduc, M., Leclerc, D., and Li, H. (2012). Crystal structure of the coat protein of the flexible filamentous papaya mosaic virus. J. Mol. Biol. 422, 263–273.